Utilization of design features of the particle telescope STEP-F and solar x-ray spectrophotometer SphinX for exploration of the Earth's radiation belt properties

Oleksiy V. Dudnik, Janusz Sylwester, Mirosław Kowaliński, Jaromir Barylak

Oleksiy V. Dudnik, Janusz Sylwester, Mirosław Kowaliński, Jaromir Barylak, "Utilization of design features of the particle telescope STEP-F and solar x-ray spectrophotometer SphinX for exploration of the Earth's radiation belt properties," Proc. SPIE 11176, Photonics Applications in Astronomy, Communications, Industry, and High-Energy Physics Experiments 2019, 111763L (6 November 2019); doi: 10.1117/12.2537296

SPIE.

Event: Photonics Applications in Astronomy, Communications, Industry, and High-Energy Physics Experiments 2019, 2019, Wilga, Poland

Utilization of design features of the particle telescope STEP-F and solar X-ray spectrophotometer SphinX for exploration of the Earth's radiation belt properties

Oleksiy V. Dudnik[a,b], Janusz Sylwester[b], Mirosław Kowaliński[b], Jaromir Barylak*[b]
[a]Institute of Radio Astronomy of National Academy of Sciences of Ukraine, Mystetstv str.,4, Kharkiv, Ukraine 61002; [b]Solar Physics Division of the Space Research Centre of Polish Academy of Sciences, Kopernika str.,11, Wroclaw, Poland 51-622

ABSTRACT

The radiation belts of the Earth and dynamics of high energy electron and proton fluxes in the magnetosphere in particular are still the target for intensive exploration by the scientific community. Quickly grown number of artificial Earth satellites including CubeSats around the Earth supports continuous improvement of the space weather forecast quality. As the charged space environment affects the wide aspects of human civilization life, the sustained monitoring of energized elementary particles is a current task. Different methods and sensors are developed to provide measurements of particle fluxes at the low Earth and geostationary orbits, at Lagrangian points and in the interplanetary space. Among them, there are silicon PIN, solid state, surface barrier detectors, organic and inorganic scintillation detectors, large area photodiodes, multi-pixelated silicon photomultipliers, etc. The gamma- and X-rays detectors are used rather often to study non-steady variations in magnetospheric particle fluxes because of a bremsstrahlung generation by precipitating subrelativistic electrons present in the upper layers of the atmosphere.

We present specific features in constructing of the Satellite Telescope of Electrons and Protons STEP-F and the solar soft X-ray spectrophotometer SphinX that allowed for discovery of some interesting phenomena in radiation belts dynamics in 2009. Technical and scientific parameters of both instruments are demonstrated as well as approaches in respective development of sensors and electronics. We present some results of data processing like detection of three-belt structure of electron fluxes, the anisotropic character of particle motion in the outer and inner belts, lower limits of the energies for particle registration by the X-ray photometer.

Keywords: satellite instrument, silicon detector, scintillator, detector head, shaping amplifier, radiation belts, energy spectrum, geomagnetic storm

1. INTRODUCTION

The CORONAS-Photon satellite was launched in January 2009 to the circular orbit with an inclination ~83^0 and the altitude of about 550 km [1]. Main tasks of the mission were the study of the hard and soft solar electromagnetic radiation and solar cosmic rays with a usage of onboard scientific equipment; the investigation of the solar activity effect in various wavelengths on the geoeffective parameters that characterize the state of the electromagnetic and radiation environments in the vicinity of the Earth [2, 3].

Most of the payload was aimed at the study of a different manifestation of solar activity. Only the two instruments were intended to monitor the high energy charged particle fluxes, i.e. the Satellite Telescope of Electrons and Protons STEP-F [4, 5, 6] and the "Electron-Pesca" detector. The soft X-ray solar spectrophotometer SphinX [7, 8, 9] in its last ADC channels, as it became clear later, was capable to detect the low and intermediate energy particle fluxes both directly and through bremsstrahlung of the primary electrons. The axes of directivity of the STEP-F and SphinX were mutually orthogonal.

In this paper, we present specific features in the design of the STEP-F and the SphinX instruments that allowed detecting some interesting phenomena in radiation belts behavior during the period of the solar activity minimum. We present also approaches in the development of sensors and electronics and main scientific parameters of both instruments.

*jbarylak@cbk.pan.wroc.pl; phone 48 71 374-76-85; fax 48 71 372-93-72; www.cbk.pan.wroc.pl

Photonics Applications in Astronomy, Communications, Industry, and High-Energy Physics Experiments 2019, edited by Ryszard S. Romaniuk, Maciej Linczuk, Proc. of SPIE Vol. 11176, 111763L
 · doi: 10.1117/12.2537296

2. THE SATELLITE TELESCOPE OF ELECTRONS AND PROTONS STEP-F

2.1 Goal and main physical parameters of the instrument

The main goal of the space experiment with the STEP-F instrument is the study of high-energy electrons, protons, and α-particles dynamics in the radiation belts of the Earth during magnetospheric storms and substorms, as well as during the influence of high-speed solar wind streams penetrating the Earth's magnetosphere [10].

Figure 1. A structural scheme of the detector head (a); the flight (b) and the breadboard (c) models of the STEP-F; the STEP-FD unit is among external detectors of the CORONAS-Photon satellite.

Table 1. Technical characteristics of the STEP-F instrument.

Parameter	Value	Remark
Mass, kg STEP-FD STEP-FE	 15.4 2.7	Weight of cable set is not included
Power Consumption, Watt STEP-FD STEP-FE	 40 8	Averaged values
Dimensions, mm x mm x mm STEP-FD STEP-FE	 337 x 395 x 293 95 x 287 x 160	
The full angle of view: degree for the lowest energies for highest energies	 108 x 108 98 x 98	Formed by conical collimator and particle stopping ranges
Active areas of detectors, cm^2 silicon matrix CsI(Tl) scintillators	 20 36, 49	 Sum of 32 elements D3, D4
Geometry factors, cm^2 x ster for the lowest energies for the lowest energies	 21.7 12.4	 Formed by conical collimator and particle stopping ranges
Temporal resolution, seconds	2, 30	12 values in each half of the minute, 24 s' collection, lasting 6 s is for transmission of outgoing frames

The other goals are the study of the influence of the electric and magnetic component variations of the Earth's magnetic field on the particle radial diffusion level in the time of the enhanced solar activity, and the study of the connection between trapped and precipitating particles of magnetospheric origin with the solar proton events and solar cosmic rays. Figure 1 represents a structural scheme, different models of the STEP-F instrument and placement of STEP-FD unit among other external units of the payload of CORONAS-Photon satellite. Table 1 represents the technical characteristics of the STEP-F device.

The STEP-F consists of the detector unit STEP-FD, mounted outside the pressurized volume of the spacecraft, and the digital signal processing unit STEP-FE, located inside the pressurized compartment. The detector unit STEP-FD consists of the detector head and 69 channels of signal analog processing. Each of the channels comprises charge-sensitive preamplifiers (CSA) and shaping amplifiers. The detector head of STEP-FD is designed as a telescopic system (Figure 1a).

2.2 Silicon matrix and scintillation CsI(Tl) detectors

The detector head contains two identical silicon position-sensitive matrix detectors D1 and D2, each of which has an area of 45 × 45 mm and a thickness of 380 micrometers, and two scintillation detectors based on a CsI(T1) single crystals viewed by the large area photodiodes in detector layer D3 and a vacuum photomultiplier in detector D4. The size of each of the 36 square elements of silicon matrix detector is 7.3 × 7.3 mm, which yields an average angular resolution of about 8° in the general field of view of the telescope for high-energy particles. Figure 2 represents common view of position-sensitive silicon PIN matrix detector, an example of resulting measurements of the one selected matrix element with the isotope ^{207}Bi conversion β-particles, and the dependence of energy resolution for the energy E=482 keV on the temperature.

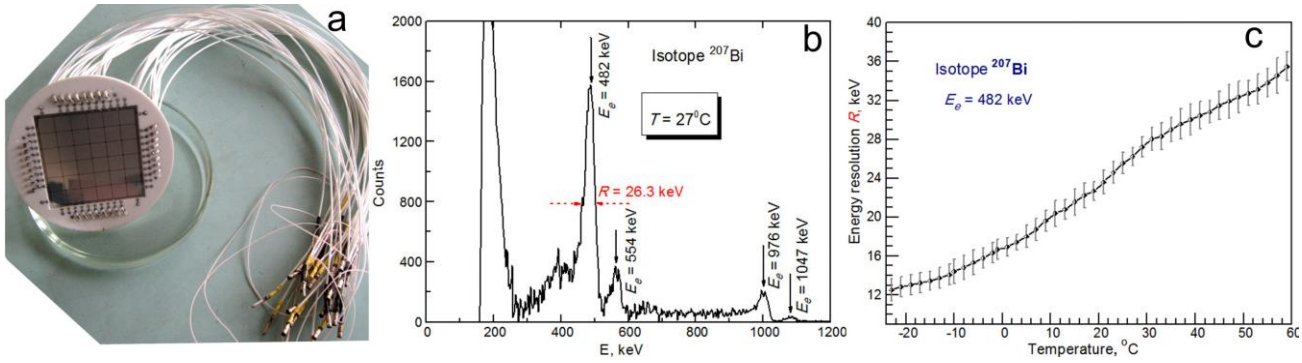

Figure 2. The position-sensitive silicon matrix detector soldered with thin coaxial cables outgoing from each matrix element (a); an example of the energy spectrum of conversion electron isotope source ^{207}Bi obtained from one matrix element at a fixed temperature (b); the resolution *R* of matrix element for the monoenergetic line E_e=482 keV of ^{207}Bi's β-particles versus temperature (c).

In Figure 3 it is shown a common view of CsI(Tl) scintillation detectors of D3 layer coupled with the silicon PIN large area photodiode of "Detection Technology, Inc." production, and example of ^{137}Cs isotope gamma-quanta energy spectrum obtained from one of the D3 layer CsI(Tl) detectors.

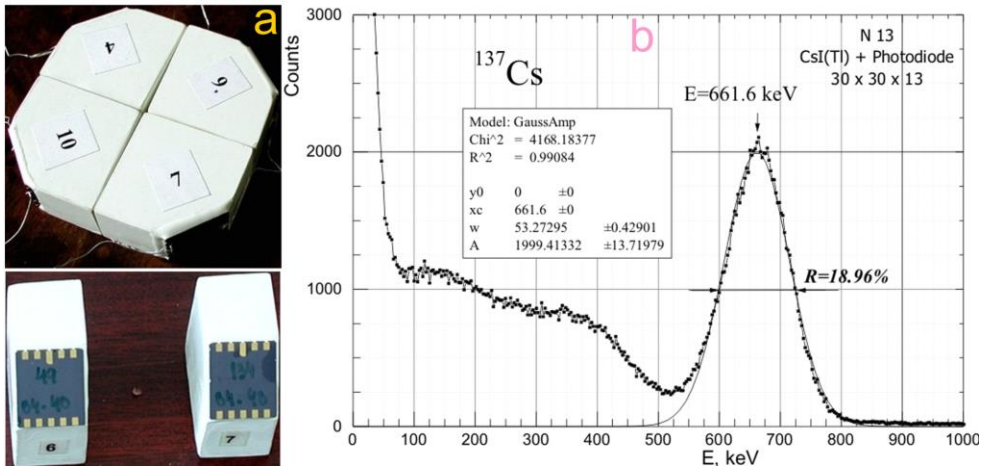

Figure 3. Scintillation detectors coupled with the large-area silicon photodiodes (a); an example of ^{137}Cs isotope gamma-quanta energy spectrum obtained from CsI(Tl) detector.

Table 2 represents the energy ranges of registered electrons, protons and channels of mixed particle registration.

Table 2. Energy ranges of registered electrons and protons.

Particle sort	Energy range	Remark
electrons	0.35 – 0.95 1.2 – 2.3 > 2.3	Provided by D2 silicon matrix detector and two first energy channels of D3 CsI(Tl) scintillator
protons	7.4 – 10.0; 15.6 – 55.2 in 9 channels; > 55.2	Provided by D2 silicon matrix detector and 10 energy channels of D3 CsI(Tl) scintillator
electrons + protons	0.18 - 0.51 (electrons) + 3.5 - 3.7 (protons)	Channel of mixed particle registration
electrons + protons	0.55 – 0.95 (electrons) + 3.7-7.4 (protons)	Channel of mixed particle registration

2.3 The analog processing of signals incoming from the detectors

Each element of the two silicon matrix detectors had own analog signal processing channel. In total, 64 channels mounted on eight printed boards served 2 x 32 elements of matrices. In such a way we reached very high relation of the

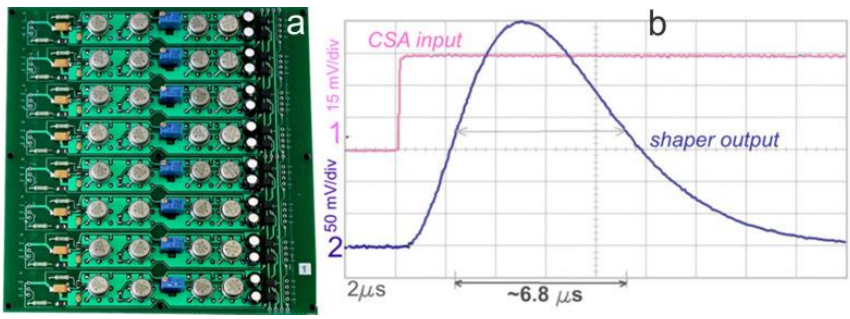

Figure 4. A view of 8-channel' printed board of analog signal processing (a); the form of shaper' output quasi-gaussian signal as a response to meander signal put into the test CSA input (b).

signal to noise so that the total active area 20 cm^2 of D1 (or D2) layer comprised electronic noises in an equivalent of one element with the area of 7.3 × 7.3 mm^2. The full width at half maximum (FWHM) of output from shapers signals is of about 6.8 microseconds (Figure 4) so that the upper limit of count rate for each element is at about $f \approx 150$ kHz. In figure 4 is shown 8-channel' printed board of analog signal processing and the form of the output signal as a response to the test meandering-type signal.

3. THE SOFT X-RAY SPECTROPHOTOMETER SPHINX

3.1 The objectives of the experiment and a brief description of the SphinX instrument

The scientific objectives of the experiment with the SphinX photometer were as follows: studies of heating processes in quiet solar corona using analysis of photon arrival time; solar soft X-ray radiation monitoring over seven orders of magnitude in intensity; determination of physical parameters of solar coronal plasma and analysis of their variability in time; identification of transient ionization effects in solar plasma in order to determine densities of flaring plasma; analysis of solar soft X-ray flux oscillations with period in the 1 – 500 seconds range; analysis of plasma chemical composition and abundance variability in solar corona for elements: Al, Ar, Ca, Fe, Mg, Si, and S.; verification of the novel, fluorescence-based, photometry measurement method; development of a reference photometric standard in soft X-rays with an absolute accuracy of 10 %. [11].

A structural scheme and a common view of the SphinX device is shown in Figure 5. SphinX was equipped with four XR-100CR detectors provided by Amptek Inc., USA. These detectors were 500 μm thick, pure silicon PIN diodes with entrance windows covered with 12.7 μm thick beryllium foil (Figure 6). Each detector also had a temperature sensor, Peltier cooler, and FET transistor inside the package. Detectors were operated in flight at temperatures below −20 °C. Detector assembly came up with one detector (D1) of entrance aperture 21.50 mm^2 (the nominal factory entrance-window area), the second one (D2) with an aperture of 0.495 mm^2 for measuring moderate X-ray fluxes, and the third (D3) with an aperture of 0.01008 mm^2 for measurements of strong flux.

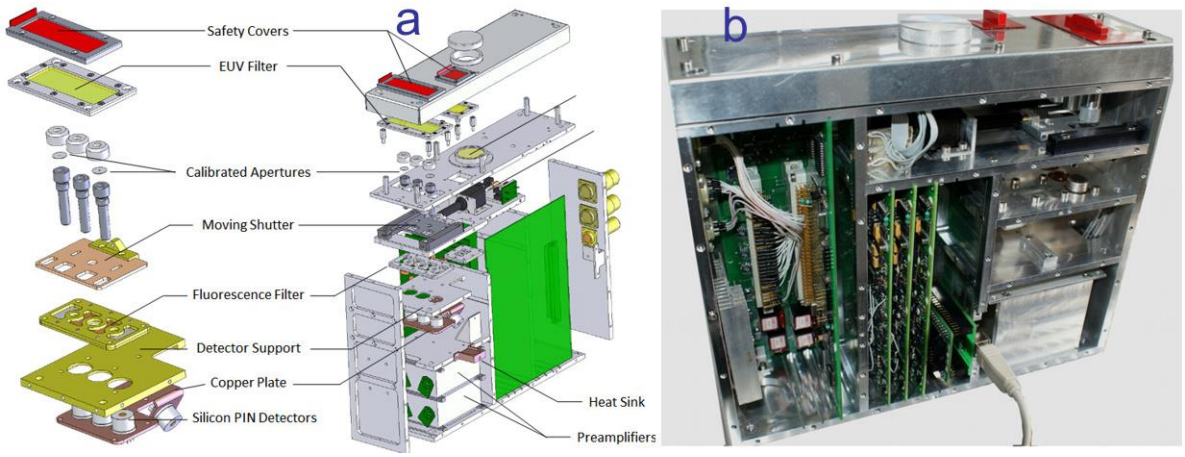

Figure 5. A detailed structural scheme (a) and a common view of the soft solar X-ray spectrophotometer SphinX (b).

3.2 Data format and characterization of the energy spectra

Each measuring channel consisted of a detector, amplifier and shaper system whose output was read by an analog-to-digital converter and sent to an on-board computer. SphinX had measured in spectral mode and event-counting mode. In the event-counting mode, every single pulse that appeared at the amplifier–shaper output was processed and information on the pulse amplitude and time of occurrence stored in memory. The pulse amplitude was converted to a channel number in the spectrometer's 256 channel space. Thus, all multichannel analyzers had 256 energy channels covering the nominal energy range of 0.0 – 15.0 keV.

Individual pulse-arrival times were determined with 1 μs accuracy. The system could distinguish and correctly measure amplitudes of two pulses occurring ≈ 6 μs one after another.

The pulses had different origins. They were produced on the output of the amplifier– shaper when an X-ray photon hit the detector crystal. The pulse amplitude was proportional to the photon energy. Pulses were also produced when energetic particles hit the detector's sensitive volume. Another source of pulses was the measurement channel electronics itself. It had to be reset every couple of seconds. After resets, additional pulses were produced at the amplifier' output. Many particle and reset-originating pulses had a large amplitude and thus are seen in the last SphinX energy channel (bin 256), which allows one to identify them.

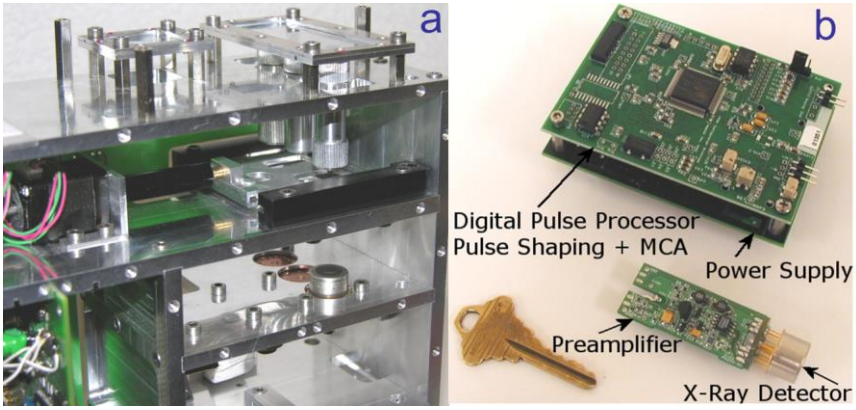

Figure 6. The sensor part of the SphinX and view of analog and digital boards of the instrument

During the mission, SphinX recorded 256-channel and ancillary broadband, 4-channel spectra (so-called basic mode spectra). The first channel of the basic mode spectra contains mainly electronic noise. In the second and third channels solar X-ray flux was recorded in the energy ranges 1.5 – 3.0 keV and 3.0 – 14.9 keV for the D1 detector and 1.0 – 3.0 keV and 3.0 – 14.9 keV for the other detectors. The last channel of the basic mode contains the events caused by energetic particles and the instrument resets (Figure 7).

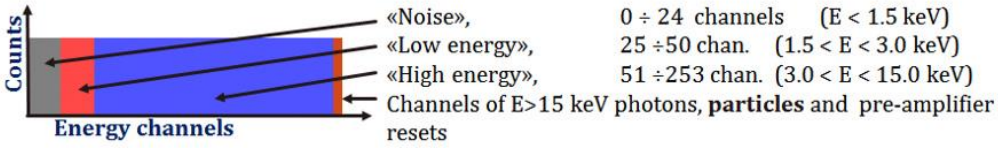

Figure 7. Structure of information from SphinX in basic mode: 256-channel' energy spectra from D1 detector.

4. SOME RESULTS OF DATA PROCESSING

4.1 Three belts structure of energetic electron fluxes in the Earth magnetosphere as measured by the STEP-F telescope

Possessing high sensitivity to low particle fluxes the STEP-F instrument detected in 2009 a three belts structure of electron fluxes in the channel of mixed particle registration (see Table 2). Figure 8 represents data with 30-seconds' temporal resolution collected on every 9th ascending nodes of satellite orbit covering latitude range from - 75^0 north to + 72^0 south over the period from May 5 to May 10, 2009. Satellite crossing of Van Allen outer and inner radiation belts is clearly seen in Southern and in Northern hemispheres. Figure 8 reveals presence of the third, additional belt being crossed by the satellite at -35 ÷ -32 degrees south, and at ~ 36 ÷ 42 degrees north. Accordingly, these latitudes correspond to McIlwain parameter $L \approx 1.6$.

The two radiation belts on $L \approx 2.28$, and on $L \approx 1.61$ were detected in the energy range $\Delta E_e = 0.18 \div 0.51$ MeV (D1e energy channel on Figure 8c) [10]. The persistent presence of the third belt on lower L-shell and the time variation

of electron population in both belts are observed depending on the overall level of geomagnetic activity. Both inner radiation belts are clearly seen at geographical longitudes that do not coincide with the South Atlantic Anomaly' longitudes [12].

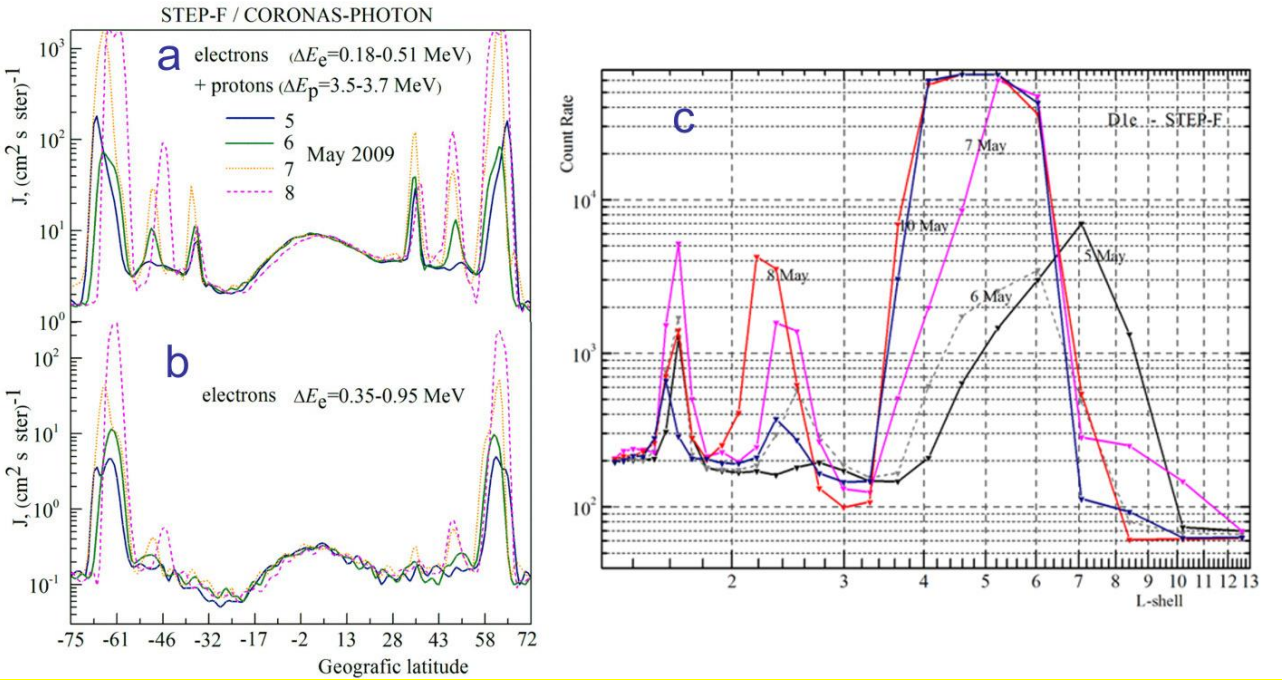

Figure 8. Particle fluxes in the channel of mixed particle registration (a) and in the electron channel of energies ΔE=0.35-0.95 MeV over the period of 5 - 10 May 2009. Different colors/lines represent individual days as indicated. c – distribution of particle fluxes by McIlwain *L*-shells.

4.2 STEP-F mapping in terms of electron fluxes in the energy range $E_e = 0.18 \div 0.51$ MeV

The satellite crossed all longitudes between $\pm 82^0$ 15 times during 24h period. This allowed us to construct daily maps of the particle content in terms of electron fluxes at the height of ~ 550 km. Results are shown in Figure 9 for the electrons of energies $\Delta E_e = 0.18 \div 0.51$ MeV on May 8, 2009, in selected color scales of particle flux densities.

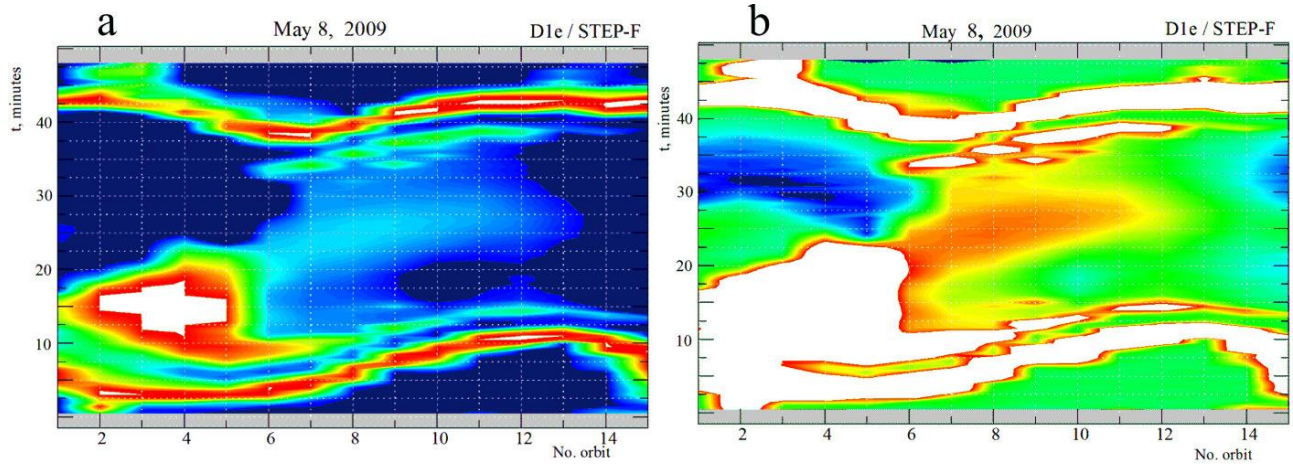

Figure 9. A map in terms of electron flux density from D1e channel measurements on May 8, 2009. The Y-axis corresponds to time phase of the semi-circle on the ascending part of satellite orbit counted from the maximum latitude in the Southern hemisphere (see the text for details).

Figure 9a represents a map of flux density of ~ 1500 particles / (cm^2 x s x ster) marked by red color, while Figure 9b represents regions with minimum fluxes where maximal flux density of ~ 15 particles / (cm^2 x s x ster) is marked also in red. It is clearly seen the global zones of enhanced particle fluxes in the South Atlantic Anomaly (SAA), in the Van Allen outer and inner radiation belts in both hemispheres, as well as the third radiation belt (from ~ 7^{th} to ~ 11^{th} orbit of the day). The specific feature of the map is the persistent presence of the enlarged electron fluxes outgoing from the SAA zone to the volume of low and near-equatorial latitudes toward the eastern longitudes.

4.3 The lower energy thresholds of electrons detected by SphinX's sensors in the SAA

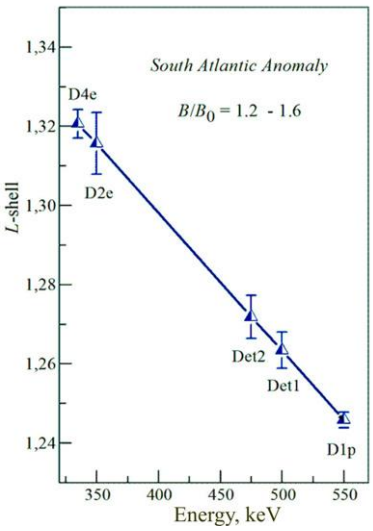

Figure 10. Dependence of averaged L-shell values corresponding to maximum electron flux densities on the particle energy.

We carried out the comparison of the data extracted from the last ADC channel of the SphinX X-ray spectrophotometer with well-calibrated STEP-F recordings. As a result, Det1 and Det2 detectors of SphinX are sensitive to electrons and the secondary γ–quanta, generated by the magnetospheric high energy electrons. The latter allowed us to introduce the concept of effective lower energy thresholds for electron registration (E_{thr1} and E_{thr2}) by Det1 and Det2 detectors, respectively [13].

The analysis of averaged over 14 days of May 2009 *L*-shell values with maximum particle count rates vs. electron energy allowed us to determine values of effective lower threshold energies E_{thr1} and E_{thr2}. We determined also the lower threshold energy of D4e channel of STEP-F, where D4 is the last, fourth in the telescopic system. In Figure 10 it is shown a dependence of *L*–shells with the largest particle fluxes, as a function of the electron energy. As a basic point the energies of D2e (electrons with energies E_e = 0.35 ÷ 0.95 MeV) and D1p (electrons with energies E_e = 0.55 ÷ 0.95 MeV + protons with energies E_p = 3.7 ÷ 7.4 MeV) energy channels of STEP-F were chosen [14].

Figure 10 demonstrates that the values of E_{thr1} and E_{thr2} are very close, assuming values ~ 500 keV and ~ 475 keV for Det1 and Det2 of SphinX, respectively. Large dispersion of these values is determined by a poor statistic (14 days analyzed), from one side, and by the diurnal displacement of the satellite position on the longitude at fixed latitude relative to the initial day.

The bottom threshold energy of D4e channel of STEP-F $E_{D4e} \approx 335$ keV as it can be seen from Figure 10. E_{D4e} values varied from day to day in the energy range from 230 to 350 keV during the period of May 1 – 14, 2009, probably due to variation of electron energy spectrum slope.

4.4 The anisotropic character of the particle motion in the bottom layers of the magnetosphere

In order to study the directivity of electron velocities the patterns were built for D1e and D2e channels of STEP-F, and for the Det1 and Det2 sensors of SphinX [15]. In Figure 11 it is shown that the satellite crossed the outer radiation belt in the Southern hemisphere at latitudes ≈ - 80 ÷ - 72 degrees south, and in the Northern hemisphere at latitudes ≈ 50 ÷ 62 degrees north (zone *1*); inner radiation belt at latitudes -62 ÷ -50 degrees south, and at ≈ 50 ÷ 62 degrees north (zone *2*); and the peripheral region of the SAA - 35 ÷ - 8 degrees south (zone *3*).

Figure 11 demonstrates almost identical electron fluxes in the outer radiation belt in both hemispheres as measured by STEP-F's D1e and D2e channels. At the same time, SphinX did not detect any substantial particle fluxes during the satellite crossing of Van Allen radiation belts in the Northern hemisphere (bottom parts of the two right-hand patterns). However, Det1 sensor observed substantially enhanced count rates in radiation belts of the Southern hemisphere. This effect is also present in the Det2 sensor of the SphinX but to a smaller extent. Taking into account the narrow field of view (~ 2^0 - 3^0) of Det1 and Det2 sensors in SphinX such tangible difference in responses on satellite crossing of the selfsame radiation belt in different hemispheres can be explained by the presence of a strong directivity in the distribution of particle velocities.

The essential distinction in counting rates derived from the SphinX's Det1 and Det2 sensors in Southern and Northern hemispheres does not correspond to almost identical count rates in both hemispheres as seen in D1e and D2e channels of the STEP-F. This fact can be explained by different angles of view of both instruments.

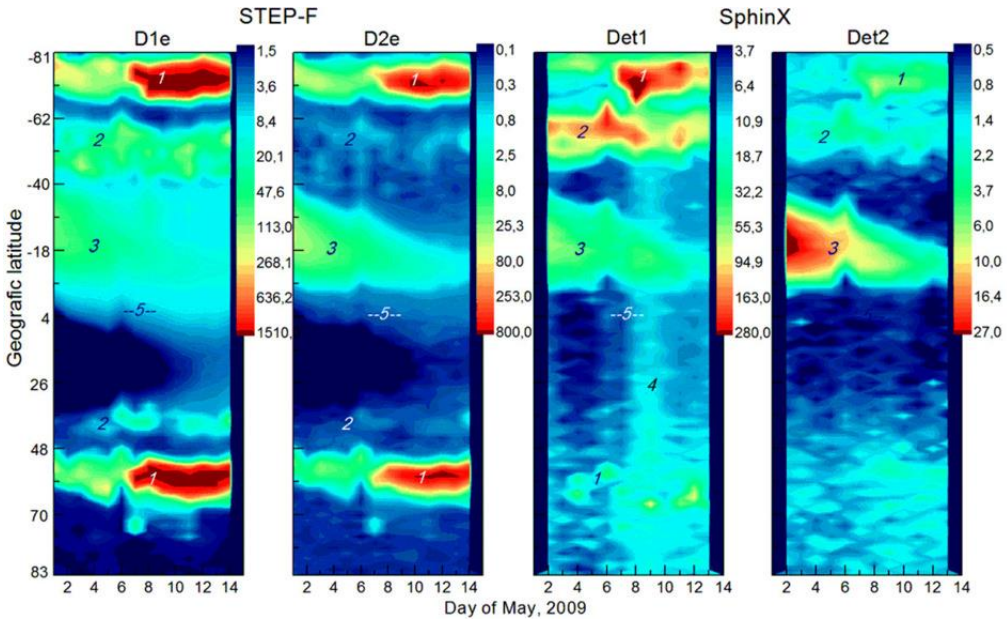

Figure 11. Patterns of particle flux variations during the period of May 1 - 14, 2009 derived from D1e and D2e channels of the STEP-F, and from Det1 and Det2 sensors of the SphinX. Regions on the plots are: 1: outer radiation belt; 2: inner radiation belt; 3: peripheral zone of the SAA; 4: particles recorded by Det1 sensor of the SphinX during the main phase of geomagnetic substorm; 5: geographic equator

Taking into account the unnoticeable level of D1 matrix detector response to the spacecraft crossing of the inner belt at the Southern hemisphere it can be concluded that SphinX's Det1 detector observed bremsstrahlung generated by magnetospheric electrons of energies with upper limit defined by the STEP-F's D1e lower threshold energy, i.e. $E_e < 180$ keV. This conclusion is additionally confirmed by records of Det1 which revealed precipitating electrons during the main phase of weak geomagnetic substorm of May 8, 2009, in a wide range of latitudes (zone *4*) including the geographic equator (zone *5*).

5. CONCLUSION

An utilization of matrix-type configuration in the first two detecting layers of the detector head of the Satellite Telescope of Electrons and Protons STEP-F allowed reaching very high ratio of the signal to noise. This led to the detection of very weak particle fluxes outside of the zones of Van Allen outer and inner radiation belts including low latitudes and near equatorial zone. Recording of the scientific information in spectral mode by the solar soft X-ray spectrophotometer SphinX allowed finding out extremely useful data in the last channel of 256-bit's records of the energy spectra on the variations of low and intermediate energies particles in the Earth's magnetosphere. Cross-analysis of data derived from both instruments led to estimating effective lower energy thresholds of primary particles registered by the SphinX sensors in a last ADC channel.

Specific features in the design of both space-based instruments enabled us to find out some new physical phenomena like existence of new one steady electron radiation belts below Van Allen inner belt, on $L \approx 1.6$ for particle energies $E \leq 500$ keV; anisotropic character of particle velocities in the Van Allen radiation belts at the heights of low Earth orbit satellites, significantly varying particle fluxes as the response to a weak substorm in the magnetosphere, and records by the SphinX photometer of precipitating low energy particles in a wide range of latitudes up to equatorial zone.

Acknowledgement

This work was supported by Polish National Science Centre grant number UMO-2015/19/B/ST9/02826.

REFERENCES

[1] Dudnik, O. V., and Zalyubovsky, I. I., "The Ukrainian Instruments Set for the Ground Accompaniment of the Joint Ukrainian-Russian Satellite Project "PHOTON" to Study the Hard Radiation of the Sun and Solar-Earth's Magnetosphere Connections", Adv. Space Res., 21**(**1/2), 343-345 (1998).

[2] Kotov, Yu. D., "Scientific goals and observational capabilities of the CORONAS-PHOTON solar satellite project", Sol. System Res., 45(2), 93-96. (2011).

[3] Dudnik, O. V., and Zalyubovsky, I. I., "Scientific tasks of international space experiment "Coronas-Photon" (in Russian)", Space Sci. Technol., 6(2/3), 3-12 (2000).

[4] Dudnik, O. V., and Malykhina, T. V., "The computer simulation of deposited energies and stopping ranges of particles in the STEP spectrometer of the Warning space project (in Russian)", Space Sci. Technol., 9(1), 15-21 (2003).

[5] Dudnik, O. V., Goka, T., Matsumoto, H., Fujii, M., Persikov, V. K., and Malykhina, T. V., "Computer simulation and calibration of the charge particle spectrometer-telescope «STEP-F»", Adv. Space Res., 32(11), 2367-2372 (2003).

[6] Dudnik, O. V., Persikov, V. K., Zalyubovsky, I. I., Timakova, T. G., Kurbatov, E. V., Kotov, Yu. D., and Yurov, V. N.. "High-sensitivity STEP-F spectrometer–telescope for high-energy particles of the CORONAS-PHOTON satellite experiment", Sol. System Res., 45(3), 212–220 (2011).

[7] Sylwester, J., Kuzin, S., Kotov, Yu. D., Farnik, F. and Reale, F., "A Fast Solar Photometer in X-rays", J. Astrophys. Astr.. 29(1-2), 339-343 (2008).

[8]. Gburek, S., Siarkowski, M., Kępa, A., Sylwester, J., Kowaliński, M., Bąkała, J., et al., "Soft X-ray variability over the present minimum of Solar activity as observed by SphinX", Sol. System Res.,. 45(2), 182–187 (2011).

[9]. Gburek, S., Sylwester, J., Kowaliński, M., Bąkała, J., Kordylewski, Z., Podgórski, P., Płocieniak, P., et al., "SphinX soft X-ray spectrophotometer: science objectives, design and performance", Sol. System Res., 45(3), 189–199 (2011).

[10] Dudnik, O. V. "Investigation of the Earth's radiation belts in May 2009 at the low orbit satellite with the STEP-F instrument (in Russain)", Space Sci. Technol., 16(5), 12-28 (2010).

[11] Gburek, S., Sylwester, J., Kowaliński, M., Bąkała, J., Kordylewski, Z., Podgórski, P., Płocieniak, S., et al., "SphinX: The Solar Photometer in X-Rays", Solar Phys., 283(2), 631–649 (2013).

[12] Dudnik, O., Sylwester, J., Podgórski, P., Gburek, S., "Radiation belts of the Earth: overview, methods of investigations, recent observations on the CORONAS-Photon spacecraft", Abstract book of Conference "Progress on EUV&X-ray spectroscopy and imaging", Wroclaw, Poland, November 20-22, 2012, 3 (2012).

[13] Dudnik, O. V., Podgórski, P., Sylwester, J., Gburek, S., Kowaliński, M., Siarkowski, M., Płocieniak, S., Bąkała, J. "Investigation of electron belts in the Earth's magnetosphere with the help of X-ray spectrophotometer SphinX and Satellite Telescope of Electrons and Protons STEP-F: preliminary Results (in Russian)", Space Sci. Technol., 17(4), 14-25 (2011).

[14] Dudnik, O. V., Podgórski, P., Sylwester, J., Gburek, S., Kowaliński, M., Siarkowski, M., Płocieniak, S., and Bąkała, J., "X-Ray Spectrophotometer SphinX and Particle Spectrometer STEP-F of the Satellite Experiment CORONAS-PHOTON. Preliminary Results of the Joint Data Analysis", Sol. System Res., 46(2), 160-169 (2012).

[15] Dudnik, O. V., Sylwester, J., Podgórski, P., "Combined study of radiation belts by the satellite particle telescope STEP-F and solar soft X-ray photometer SphinX during recent deep minimum of solar activity", Program and Abstract Book of 23rd National Solar Physics Meeting, Liptovský Mikuláš, Slovakia, 30 May-3 June 2016, 11 (2016).